








Cite this: DOI: 10.1039/d1lc00082a

Size-tuneable isolation of cancer cells using stretchable inertial microfluidics

 Hedieh Fallahi,  Sharda Yadav, Hoang-Phuong Phan,  Hang Ta, 
 Jun Zhang * and Nam-Trung Nguyen *

Inertial microfluidics is a simple, low cost, efficient size-based separation technique which is being widely investigated for rare-cell isolation and detection. Due to the fixed geometrical dimensions of the current rigid inertial microfluidic systems, most of them are only capable of isolating and separating cells with certain types and sizes. Herein, we report the design, fabrication, and validation of a stretchable inertial microfluidic device with a tuneable separation threshold that can be used for heterogenous mixtures of particles and cells. Stretchability allows for the fine-tuning of the critical sorting size, resulting in a high separation resolution that makes the separation of cells with small size differences possible. We validated the tunability of the separation threshold by stretching the length of a microchannel to separate the particle sizes of interest. We also evaluated the focusing efficiency, flow behaviour, and the positions of cancer cells and white blood cells (WBCs) in an elongated channel, separately. In addition, the performance of the device was verified by isolating cancer cells from WBCs which revealed a high recovery rate and purity. The stretchable chip showed promising results in the separation of cells with comparable sizes. Further validation of the chip using whole blood spiked with cancer cells delivered a 98.6% recovery rate with 90% purity. Elongating a stretchable microfluidic chip enables onsite modification of the dimensions of a microchannel leading to a precise tunability of the separation threshold as well as a high separation resolution.

 Received 1st February 2021,
 Accepted 31st March 2021

DOI: 10.1039/d1lc00082a

rsc.li/loc

Introduction

Sorting and isolation of biological cells have many applications in both clinical applications and fundamental research. Circulating tumour cells (CTCs) are among the rare cells that can be isolated from the blood stream and provide a plethora of information in assessing the prognosis or diagnosis of metastatic cancers as well as monitoring therapeutic responses to treatments.^{1–6} Although CTCs are rare cells with as few as 1 to 10 cells per millilitre of peripheral blood,⁷ they are highly valuable biomarkers for cancer evaluation.¹ For instance, CTC detection promises cancer screening and early diagnosis,⁸ risk stratification⁹ and prognostication in the early stages of cancer.¹⁰ Identification of CTCs also plays an important role in monitoring responses to therapy,¹¹ cancer progression,¹² and detection of minimal residual disease.¹³ CTC detection is also beneficial to fundamental research, providing insight into treatment resistance. Furthermore, in cases where the tissue biopsy is not possible due to the location of the tumour or when the

tumour could not be identified or located, CTC analysis is crucial for cancer diagnosis.¹⁴ Cancer cells spiked into blood cells have been widely used to mimic the CTCs in blood.^{14–18}

Microfluidics has been one of the mainstream technologies that enable the efficient isolation and analysis of CTCs.^{19–21} Among numerous microfluidic platforms, inertial microfluidics is a promising tool that has been utilized to focus, sort and separate biological particles including CTCs.^{22,23} Inertial microfluidic technologies take advantage of the physical differences between CTCs and their surrounding cells to isolate and detect them. Inertial microfluidics is superior to other microfluidic platforms in terms of design simplicity, being passive and no requirement for external force, precision, low cost, and high throughput.²⁴ Among the reported inertial microfluidic platforms for rare cell isolation, multi-flow straight microchannels showed promising results.^{25–33} Multi-flow inertial microfluidics with straight channels have been reported to have high recovery ratios and throughputs, but still lack tunability due to the fixed geometry.³⁴

Particle size is the basis of the inertial microfluidic sorting and separation.³⁵ As size-based separation is determined by the geometry of the microfluidic platforms, once a device has been manufactured, it cannot not be altered so the device

Queensland Micro- and Nanotechnology Centre, Griffith University, Nathan, Queensland 4111, Australia. E-mail: jun.zhang@griffith.edu.au, nam-trung.nguyen@griffith.edu.au

cannot be used for sorting and separation of particles of varying sizes. In other words, every inertial microfluidic device has a certain separation threshold that is mostly influenced by the dimensions of the device. To adjust the separation threshold and optimise the separation performance, iterative design, fabrication, and testing are often required, which is time consuming, labour intensive and cumbersome.

Several attempts were made to develop methods that can tune the separation threshold of inertial microfluidic devices. Papautsky's group studied the effect of flowrates, flowrate ratios, and the channel resistance ratios on the separation threshold of a co-flow straight microchannel.³⁶ Although these parameters influence the separation threshold, the coupled effects of these factors complicate the determination of these parameters when tuning the separation threshold. Furthermore, manipulation of the separation threshold of the device on a smaller scale may not be feasible. Moreover, there is an absolute need for the redesign and refabrication of new devices for microparticles of varying sizes. Zhou *et al.* studied the migration dynamics of the cells in a co-flow rectangular microchannel.³⁷ The team demonstrated that a precise control of the channel length could enhance the separation efficiency. However, the channel length of a fabricated rigid device was not tuneable. Lee group reported a new geometry that can focus particles with different sizes at corresponding locations by changing the inflection points of the velocity profile and the fluid viscosity.^{38,39} However, this approach requires a complex design, and complicated fabrication steps. Furthermore, testing different dimensions and channel shapes are unavoidable. Zhou *et al.* utilized non-Newtonian viscoelastic fluids to implement elasto-inertial separation.⁴⁰ The relatively high viscosity of non-Newtonian fluids leads to lower throughputs, requiring high driving pressure, and generating a higher pressure drop that may result in device failure.⁴¹ Considering all the drawbacks associated with methods reported to date on tuneable inertial microfluidics, real tunability of an inertial microfluidic device is still not available.

We recently reported a novel stretchable inertial microfluidic device that improves the focusing and separation efficiency of a binary mixture of particles.⁴² Flexibility and stretchability of a microfluidic device allows for changing its dimensions accordingly,⁴³ opening up new capabilities with broad applications particularly in the emerging field of micro elastofluidics.⁴⁴ Stretching has also been implemented for early cancer detection as a technique to induce more biomarkers.^{45–47} This paper reports on the use of stretchable inertial microfluidics to obtaining a tuneable threshold for particle separation and applies it to the isolation of cancer cells from blood. The novelty of this works lies in its ability to dynamically adjust the device dimensions providing a tuneable separation threshold as well as a high separation resolution, and consequently allowing for separation of cancer cells with a broad size range as well as small size difference.

Using a mixture of particles with a continuous size distribution, we demonstrated that the separation threshold can be precisely controlled. The device can focus particles of desired sizes by stretching the chip to a corresponding length. Next, we demonstrated focusing enhancement of cancer cells and the migration behaviour of white blood cells (WBCs) in an elongated channel. Subsequently, we showed that this stretchable microfluidic device can isolate cancer cells spiked into WBCs with a high recovery rate. Furthermore, cancer cells were spiked into diluted whole blood. The tunability of separation threshold was investigated under elongation and demonstrated in very high recovery rates without compromising the purity. A unique feature of our proposed concept with respect to standard microfluidic platforms is the ability to isolate smaller cancer cells with similar sizes to WBCs. This stretchable technique brings about the opportunity of applying minute changes to the dimensions of the channel to gain a great performance enhancement. Our novel technique with a large separation resolution offers interesting opportunities to separate a variety of cell sizes of interest without iterating the design, fabrication, and optimization processes.

Materials and methods

Device fabrication

Flexible and stretchable microfluidic chips were fabricated following the procedure reported in our previous work.⁴² Briefly, a 4-inch silicone mold was fabricated using SU-8 3050 (MicroChem Corp.) photoresist by conventional photolithography. Microchannels and stretchable layers were fabricated by soft lithography using poly(dimethyl siloxane) (PDMS) (Sylgard 184, Dow Corning) and the curing agent with a ratio of 10 : 1. The PDMS layers were cured in an oven for 2 hours at 75 °C followed by surface treatment with a plasma cleaner (PDC-32G-2, Harrick Plasma) and subsequent bonding. Thick PDMS slabs were then bonded to the top and bottom of the chip at the inlet and outlet areas for supporting the tubing as well as giving structural reinforcement to the whole device. Inlets and outlets were punched manually and connected to external tubing. The channel dimensions are 10 mm in length, 100 µm in width and 45 µm in height. The microchannel has two inlets to introduce the sample and the buffer flows. The end of the channel is connected to a trifurcation region with a middle channel, also called centre channel, leading to the target outlet for focusing the large particles and two other side channels directing to waste outlet for collecting the smaller particles. The chip was then clamped in a custom-made stretching platform, using a design that was reported in our previous work.⁴² The custom-made stretching platform is made by assembling laser machined poly(methyl methacrylate) (PMMA) parts to an off-the-shelf micrometre translation stage. Fig. 1a illustrates the schematic of the stretchable microfluidic chip placed in the custom-made stretching platform. The separation mechanism is

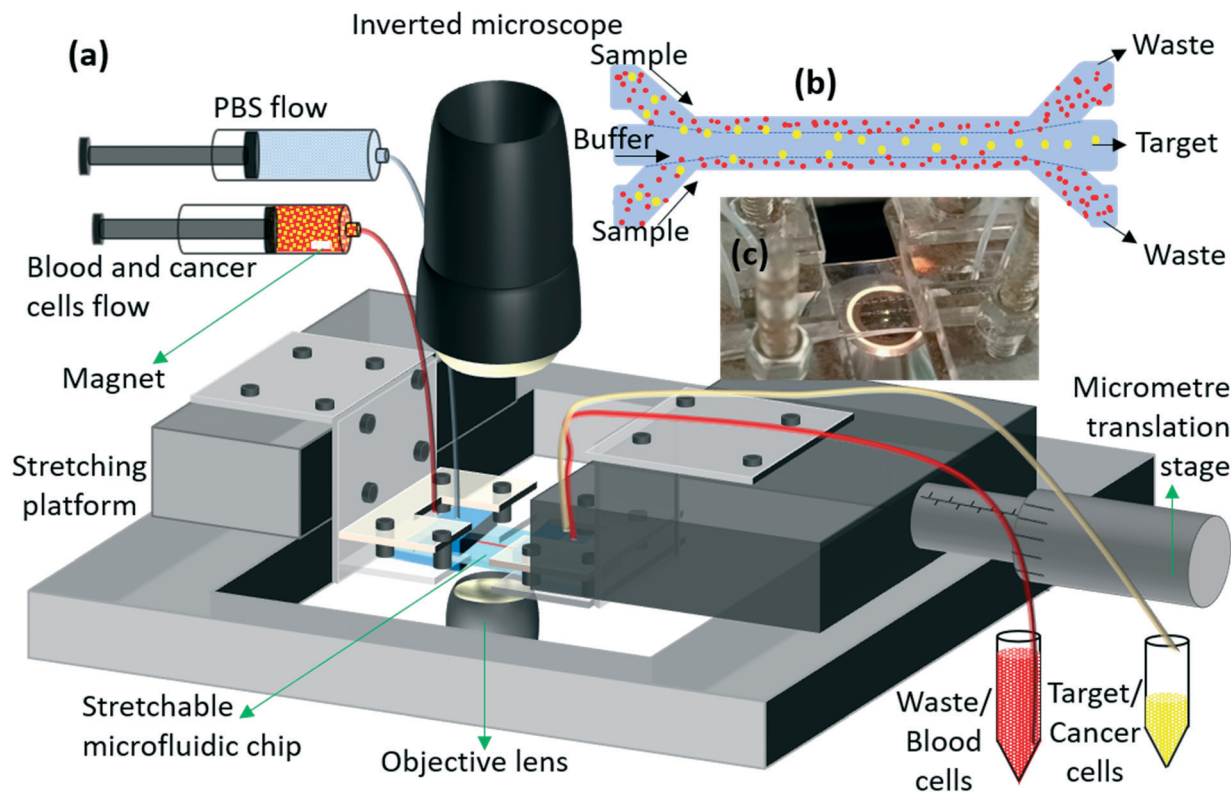


Fig. 1 Schematic setup of the stretchable microfluidic device and the custom-made stretching platform. (a) Set up is placed on the stage of an inverted microscope, sample and buffer are infused into the device at specific flowrates, the chip is stretched using the customized micrometre translation stage and the target cancer cells are isolated and collected in one tube while the normal blood cells are collected in a separate tube. (b) Configuration of the multi-flow straight microchannel and the position of the cancer cells and the blood cells along the channel downstream. (c) The actual stretchable microfluidic chip under elongation.

demonstrated in Fig. 1b. Fig. 1c shows the actual image of the elongated microfluidic chip.

Experimental setup

Sample and buffer flows were delivered to the chip using a syringe pump (neMESYS, Centoni GmbH) to maintain constant flowrates of 10 and 200 $\mu\text{L min}^{-1}$ for the sample and the buffer flows, respectively. To avoid particle/cell precipitation, the sample was stirred continuously using a small magnetic stirring bar placed inside the syringe. The outputs were collected in 1.5 mL microcentrifuge tubes. The whole setup was placed on the stage of an inverted microscope (Nikon Eclipse Ti) equipped with a high-speed camera (Phantom Miro3, Vision Research) to monitor and record the flow of the samples inside the microchannels. An average of 3000 frames were stacked together using ImageJ® (NIH, USA) to visualize the positions and the trajectories of the samples.

Microparticle sample preparation

We first used poly(methyl methacrylate) (PMMA) beads with a continuous size distribution of 2–26 μm (Cospheric LLC, Santa Barbara, CA, USA) to characterize the tunability of separation threshold through elongating the chip. A saline

buffer solution of 40 g NaCl, 200 mL deionized water, and 200 μL Tween20 was prepared as the buffer/sheath flow and was also used for preparing the particle solutions. NaCl and Tween20 prevent sedimentation and aggregation of the particles, respectively. 67 mg of the particle powder was dissolved in 25 mL of the prepared saline buffer and stirred well to obtain a uniform suspension.

Blood and cell sample preparation

Blood cells and cancer cells were introduced to the device to evaluate the focusing and separation efficiency of the device. Human whole blood was obtained from Australian Red Cross Lifeblood (Brisbane, Australia) under the Material Supply Deed number 20-02QLD-11. The ethics approval was obtained from Griffith University/University of Queensland (Approval number: 2020/233 and 2015001037). T47D cancer cells (human breast cancer) were provided from American Type Tissue Culture (ATCC, Manassas, VA, USA). Cancer cells were cultured in humidified atmosphere at 37 $^{\circ}\text{C}$, 5% CO_2 using Dulbecco's modified eagle medium/Nutrient Mixture F-12 (DEME/F12), 10% heat-inactivated fetal bovine serum (FBS), and 1% penicillin/streptomycin. All cell culture reagents were obtained from Gibco-Thermo Fisher Scientific (Waltham, MA, USA). Cancer cells were harvested and then stained with

Mitotracker Green FM, which was purchased from Thermo Fisher Scientific (Eugene, OR, USA). At first, the harvested cancer cells were centrifuged to obtain a cell pellet. After aspirating the supernatant, the cancer cells were resuspended in staining solution followed by a 30-minute incubation. Next, the cancer cells were re-centrifuged to collect the pellet and were later spiked into the blood sample. Cell counting was performed using a haemocytometer (BRAND® counting chamber BLAUBRAND® Neubauer improved). White blood cells (WBCs) were isolated using a density gradient medium (Leuko Spin Medium, pluriSelect Life Science UG & Co. KG) according to the protocol provided by the company. Briefly, the blood sample was diluted and carefully layered on top of the density gradient medium. The prepared sample was then centrifuged at $1000 \times g$ for 30 minutes. The leukocyte cell fraction was removed from the medium and the collected WBCs were washed twice before use. Both WBCs and whole blood were diluted with phosphate buffered saline (PBS) (Thermo scientific) and were later respectively spiked with stained cancer cells in order to characterise the separation performance of the device for cancer cell isolation.

Sizing and counting

To analyse the output samples of the experiments, we used an inverted microscope (Nikon Eclipse Ti2) equipped with an LED illumination source (pE-4000, CoolLED) for fluorescence microscopy. Particle size distribution was quantified based on the images taken from the output samples under the microscope. During each run of the experiment under a given stretching length, the outputs of each outlet were collected in tubes for a certain period of time. Then, we centrifuged the collected samples and discarded the supernatant for having a concentrated sample for subsequent analysis. A drop of each sample was placed on a clean microscope slide and covered by a glass slip. Using a $40\times$ magnification of the microscope, high resolution images from different areas of the samples were recorded. These images were analysed using ImageJ® for size determination. Around 700 particles were studied for each sample to obtain the size distribution. Cell counting was performed using the images taken from a haemocytometer under the microscope. $10\times$ magnification images were taken using the microscope to later conduct the automatic counting using ImageJ®. Total cells and stained cancer cells were counted under brightfield and fluorescence modes of the microscope, respectively.

The performance of the stretchable chip was quantified with the following parameters: (i) focusing efficiency (*i.e.* the number of the focused particles/cells located in the $20 \mu\text{m}$ proximity of the centre line of the microchannel over the total number of particles/cells); (ii) recovery rate or the separation efficiency of the target cells in the middle outlet (*i.e.* the number of target particles/cells collected from the middle outlet over the total number of the target particles/cells collected from all outlets); (iii) rejection ratio or the separation efficiency of the non-target/waste cells in the side

outlets (*i.e.* the number of waste cells collected from the side outlets over the number of waste cells collected from all outlets); and (iv) purity (*i.e.* the ratio of target cell number to total number of cells collected from the middle outlet).

Results and discussion

Physics of inertial separation

In our stretchable co-flow microfluidic chip, sorting and separation mechanism is based on the inertial forces applied on the randomly dispersed particles that enter the microchannel. Two main forces are applied on the particles: (i) drag force (F_D) that leads to the movement of the particles along the streamlines, and (ii) lift force (F_L) that is the cause of the lateral migration of the particles across the streamlines and consists of two components, shear-induced lift force and wall-induced lift force.³⁵ The final equilibrium position of the microparticles inside a microchannel is where the shear induced lift force and the wall induced lift force balance each other. Inertial lift force is a function of the size of the particles as well as the geometry of the microchannel. The larger the particle size, the faster they travel laterally and focus to the centre of the microchannel, while the smaller particles are subjected to less forces and need more time to travel toward the centre. As such, while the bigger particles arrive at the centre, the smaller ones still remain close to the channel sidewalls, subsequently enabling size-based inertial separation, Fig. 1b. The timing of the occurrence of the above phenomenon is critical and is a function of the geometry of the microchannel, mainly the length. Therefore, each microfluidic device has to be designed for sorting and separating a given narrow range of particle sizes and cannot be used for broad size ranges.

Separation threshold, also termed cut-off size, is the size above which, particles exit through the target outlet and below which particles are collected from the waste outlets. Cut-off size is an important parameter as it determines separation efficiency and purity of the target particles or cells. For straight microchannels, the cut-off size is fixed as it is dependent on the geometry of the channel. Consequently, there should be a well-defined size difference between the particles to be separated. However, biological samples are heterogeneous microparticles with a broad distribution of sizes and may have similar sizes to the other particles to be separated from. Therefore, a system that can precisely tune the cut-off size of the microchannels onsite based on different particle sizes is desired.

Evaluation of the tunability of the cut-off size and separation resolution in an elongated channel

We introduced a heterogeneous mixture of microparticles of continuous sizes ranging from 2 to $26 \mu\text{m}$ into the stretchable microfluidic device to study the tunability of the channel cut-off size under different stretching conditions. From the other inlet the buffer was infused to the chip. The flowrate ratio (FRR) is defined as the ratio of the sample

flowrate to the buffer flowrate. For all the experiments in this paper, the flowrate ratio was set at $10/200 \mu\text{L min}^{-1}$. The high buffer flowrate dilutes the sample and therefore makes the use of more concentrated samples possible. In addition, this high flowrate pushes the particles/cells tightly to the sides and allows for high-resolution separation of the cells. To get detailed data on size distribution at each stretching length, we evaluated over one thousand particles from each output. The cut-off size was quantified as the size at which 80% of the microparticles exit through the target outlet.

Fig. 2a–d show the distribution of particle sizes exiting through the target and side outlets under different stretching lengths. The distributions represent the percentage of each particle size exiting through the target and side outlets. Without stretching, the cut-off size was $18 \mu\text{m}$ as more than 80% of the $18 \mu\text{m}$ particles were collected from the target outlet. By stretching the channel along its longitudinal

direction, the cut-off size decreased slightly and continuously. This is a desirable behaviour, because we do not want a sudden change in cut-off size as the particle sizes to be separated could be very close. Fig. 2e plots the particle size distribution of the middle outlet for different stretching lengths, which clearly indicates that the cut-off size decreases from $18 \mu\text{m}$ to approximately $15 \mu\text{m}$ by elongating the channel. According to our earlier work, elongating the microchannel reduces the height and the width of the rectangular cross section. However, the aspect ratio δ remains constant with channel elongation. These deformations lead to an increase in the lateral displacement ratio θ that is the ratio of the particle lateral displacement to the channel width.⁴² We derived the following equation for θ where d_L is the lateral displacement of the particles, a is the particle diameter, L is the channel length, Q is the flowrate and W is the width of the channel.

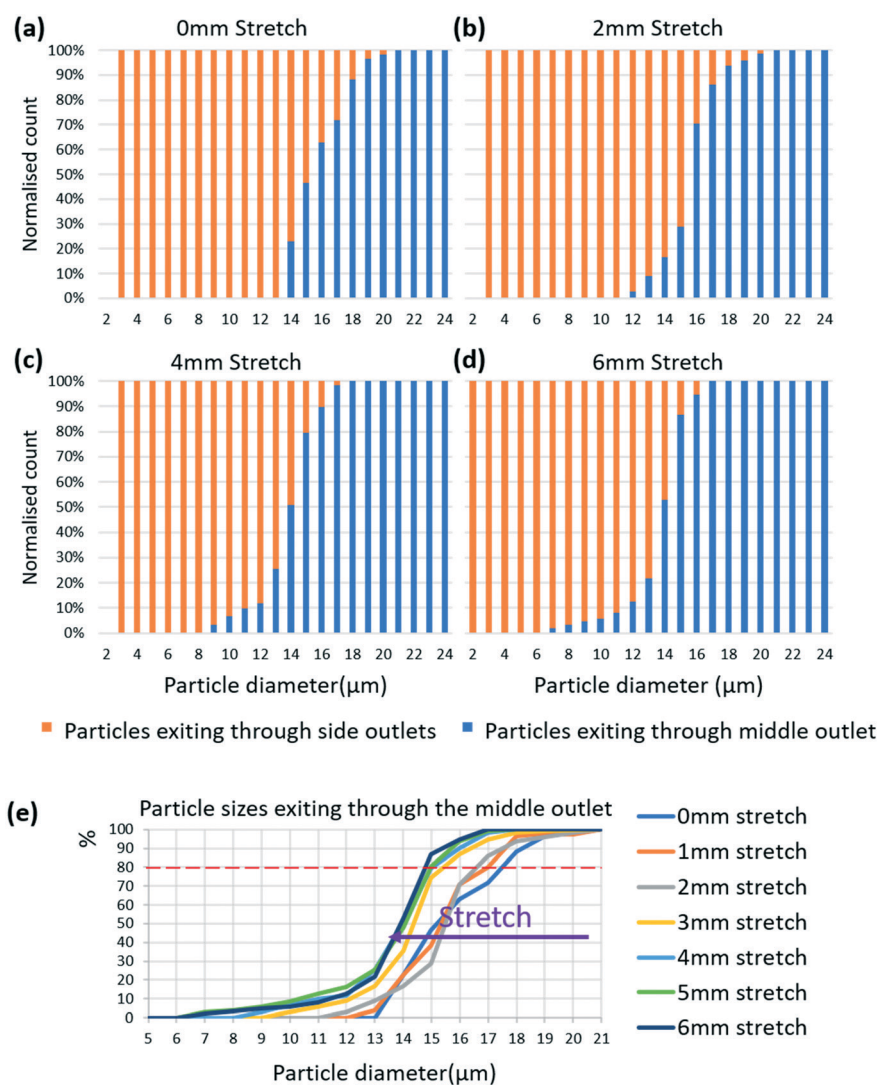


Fig. 2 Tunability of the microchannel cut-off size for a heterogeneous mixture of different sized particles under different stretching lengths: (a) to (d) the size distributions of particles exiting the middle and side outlets under different stretching lengths. (e) Size distribution at the middle outlet demonstrating that stretching reduces the cut-off size.

$$\theta = \frac{d_L}{W} \propto \frac{a^2 L Q^{\frac{1}{2}}}{W^{\frac{3}{2}}} \quad (1)$$

According to eqn (1), elongating the channel reduces the width and consequently increases θ . As such, stretching assists the particles/cells in reaching their final equilibrium position relatively faster. Therefore, a shorter downstream distance is required for the particles/cells to focus while under stretching. Furthermore, Fig. 2e indicates that by stretching the channel, more particles larger than the cut-off size exit through the middle outlet. Thus, recovery ratio (separation efficiency) of particles with sizes above the cut-off size can be improved by stretching.

Separation resolution is an important specification representing the ability of an inertial microfluidic device for accurately separating particles of varying sizes. The separation resolution is defined as the smallest size difference between the particles separated with high efficiencies. So far, the highest separation efficiencies reported are for particles with size differences of $<2 \mu\text{m}$, which is for triangular cross-section microchannels⁴⁸ and spiral microchannels with trapezoidal cross-sections.⁴⁹ Furthermore, Lee *et al.* have reported remarkably high separation resolutions by using a contraction–expansion array (CEA) which has a complicated fabrication procedure.⁵⁰ Wang *et al.* defined separation resolution (R_s) as the average diameter (a) of the particles to be separated divided by the smallest difference in diameter that can be separated in a microfluidic device (Δa).⁵¹ According to this method, the separation resolution for our heterogenous mixture of particles (2–26 μm), is around 14. This is a very high resolution for separating particles with 1 μm variation in size and the relatively high efficiency of over 80%. This resolution is much higher than previously reported, which typically range from 5–10.^{48,49,51} The high separation resolution is due to the stretchable nature of our inertial microfluidic device, allowing for a minute change to the dimensions of the microchannel and for fine-tuning of the cut-off size.

Focusing enhancement of cancer cells in an elongated channel

Cells exhibit different behaviour from microparticles in a microfluidic device due to their different densities as well as cell–cell interactions. However, as long as the sample is sufficiently diluted to be considered as a Newtonian fluid, inertial migration is still the dominant phenomenon in the microchannel. As such, to assess the focusing behaviour of the cancer cells in the stretching microfluidic chip, T47D cancer cells with a concentration of 1×10^6 count per mL were delivered into a 10 mm long microchannel from the centre inlet, while PBS was infused from the side inlet. Our cultured T47D cancer cells had a size range of 12–27 μm with the majority of them around 16–19 μm . The FRR was the same as the one in the particle separation experiments. Focusing efficiencies of the cancer cells at each stretching

length were calculated as 66.4%, 71.9%, 74.81%, and 77.9% for 0 mm, 2 mm, 4 mm, and 6 mm stretching lengths, respectively. This enhancement was resulted from the changes in the dimensions including a longer length and a smaller width that lead to a decreased cut-off size of the middle outlet. Therefore, with stretching, smaller cancer cells could also focus toward the channel centre line. It needs to be noted that since the channel expands at the trifurcation area, not all the cells need to be focused to the centre line to exit through the middle outlet. Thus, cells close to the centre line are also collected from the target outlet. Fig. 3 shows the distribution of cancer cells at the trifurcation area of the microchannel at different elongations. Without stretching, a large part of the cancer cells had migrated to the centre, Fig. 3a. This is because the channel length of 10 mm is already long enough for cell sizes of 18 μm and above to travel to the centre. By stretching the channel, more cancer cells migrate to the centre of the microchannel, Fig. 3b–d. To quantify this observation, we calculated the percentage of the cancer cells collected from the centre outlet and showed them on the corresponding images of Fig. 3.

Migration of WBC in an elongated channel

To study the migration of the WBCs under stretching, isolated WBCs (3×10^6 count per mL) and PBS were infused to the 10 mm long stretchable device from the middle and side inlets, respectively. Fig. 4a–d show the migration behaviour of the WBCs under stretching. For a better evaluation, we calculated the percentage of the WBCs that go into the middle outlet based on the videos recorded from the trifurcation area and indicated them on the corresponding images of Fig. 4. Without stretching, most of the WBCs travel

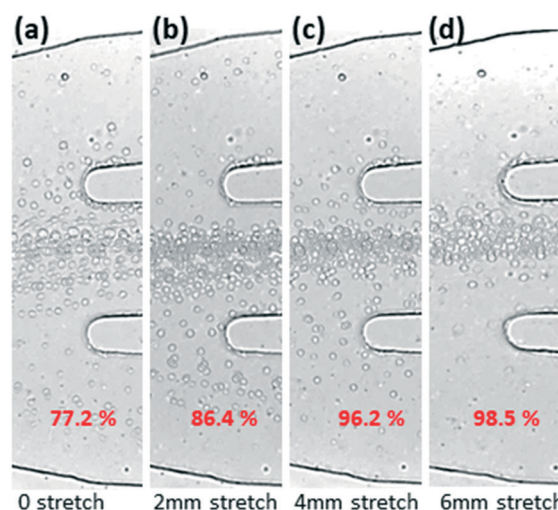


Fig. 3 Stacked brightfield images of the trifurcation area of a 10 mm long channel at different elongations. Figures (a) to (d) demonstrate that stretching the chip increases the focusing efficiency and the enrichment of the cancer cells in the centre outlet. Red numbers on each image represent the percentage of the cancer cells collected from the centre outlet.

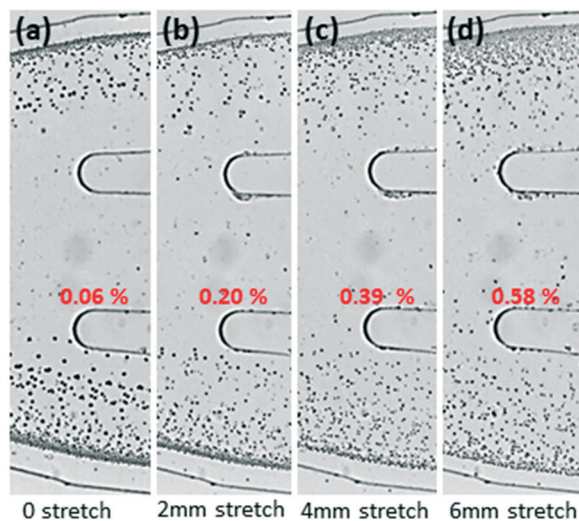


Fig. 4 Demonstration of WBC flow at the expanding region of a 10 mm long microchannel under different stretching lengths. From (a) to (d) by increasing the elongation, few WBCs migrate to the centre and contaminate the middle outlet. The red digits indicated on each image, show the percentage of the WBCs migrated to the centre of the microchannel for the corresponding stretching length.

through the sides and only 0.06% of the WBCs flow through the middle outlet, Fig. 4a. Under stretching, a few larger WBCs moved away from the walls and approached the centre, Fig. 4b–d. However, most of the WBCs could not migrate laterally far enough to enter the middle outlet. Only very few WBCs could reach to the middle outlet. At 6 mm stretching length, only 0.58% of the WBCs were collected from the middle outlet, Fig. 4d. The WBCs in our experiments had sizes ranging from 8 to 16 μm with majority of them around 8 to 10 μm . As the large part of the WBC sizes are under 10 μm , which is far below the cut-off size of any stretching length in our experiments, the WBCs are not subjected to enough inertial forces to focus them to the centre of the microchannel. However, very few WBCs sized over 14 μm contaminated the middle outlet at higher stretching length due to the reduction of the cut-off size.

Isolation of spiked cancer cells from WBCs in an elongated channel

The major objective of our stretching platform is to isolate the cell sizes of interest, particularly when there is a size overlap of the cells to be separated. The T47D cancer cells (12 to 27 μm) have a size overlap with WBCs (8 to 16 μm), therefore adjusting the separation threshold and achieving a high separation resolution is critical to achieve a good isolation of the cancer cells. However, this is challenging by using conventional inertial microfluidic devices. We demonstrated the tuneable isolation of cancer cells using the proposed stretchable inertial microfluidic device. We spiked 50 μL of cancer cells suspension (1×10^6 count per mL) into 2 mL of WBCs (3×10^6 count per mL). The spiked WBCs and PBS buffer were separately flowed through the centre and

side inlets. Processed samples at the outlets were collected for each stretching length and the concentrations of cancer cells and WBCs were measured at each run.

Fig. 5a–d show the trifurcation area of the channel under different stretching lengths. Without stretching, a large part of the cancer cells (approximately 71%), with sizes larger than 17 μm were isolated and collected from the target outlet. The remaining 29% of the cancer cells including the ones smaller than 18 μm were collected from the side outlets. Stretching the channel reduced the cut-off size of the middle outlet, and more cancer cells with irregular shapes focused to the centre which resulted in the isolation of the smaller cancer cells through the centre outlet. Therefore, the recovery rate of cancer cells increased continuously even more than 95% when stretching length is 6 mm, Fig. 5m. Fig. 5e–h show the fluorescence images of the stained cancer cells collected from the target/middle outlet at 0, 2, 4, and 6 mm stretching lengths. Clearly, more cancer cells were isolated under stretching. Fig. 5i–l show the cancer cells obtained from the waste/side outlets. Stretching allows more cancer cells with smaller sizes to flow through the middle outlet, and less to exit through the side outlets. Fig. 5m shows the recovery rate and purity of cancer cells as well as the WBC rejection ratio. Elongating the channel for a total of 6 mm increases the recovery rate of the cancer cells from 71% to 97.4%, while the purity is reduced from 90.9% to 82.6%. Considering that the concentration of WBCs is ~ 120 times higher than that of cancer cells at the inlet and that some T47D cancer cells have similar sizes to that of WBCs, the purity of 82.6% is regarded a promising outcome owing to the capability of onsite tuning the length and finding its optimum. WBC rejection ratio (99.7% at 0 stretch) did not change significantly by elongating the channel length (98.2% at 6 mm stretch), which demonstrates another advantage in using a stretchable microfluidic chip.

Isolation of spiked cancer cells from diluted whole blood in an elongated channel

WBCs account for only 1% of the whole blood, while other components smaller than WBCs constitute the bulk of the blood. However, whole blood is not a Newtonian fluid which makes it greatly challenging to work with in an inertial microfluidic device. For non-Newtonian fluids, inertial forces may vary, leading to a different focusing behaviour. The cell–cell interactions also become more dominant in the whole blood flow. Thus, whole blood needs to be diluted to mitigate the effects of cell–cell interactions and non-Newtonian fluid properties. According to the literature, a 50 \times dilution rate offers a relatively good cell focusing performance.⁵² Therefore, we diluted the whole blood by 50 \times , followed by spiking it with T47D cancer cells. The concentration of cancer cells in diluted blood was 1.25×10^6 count per mL. FRR, sample and buffer delivery conditions, and stretching lengths were the same as the above experiments.

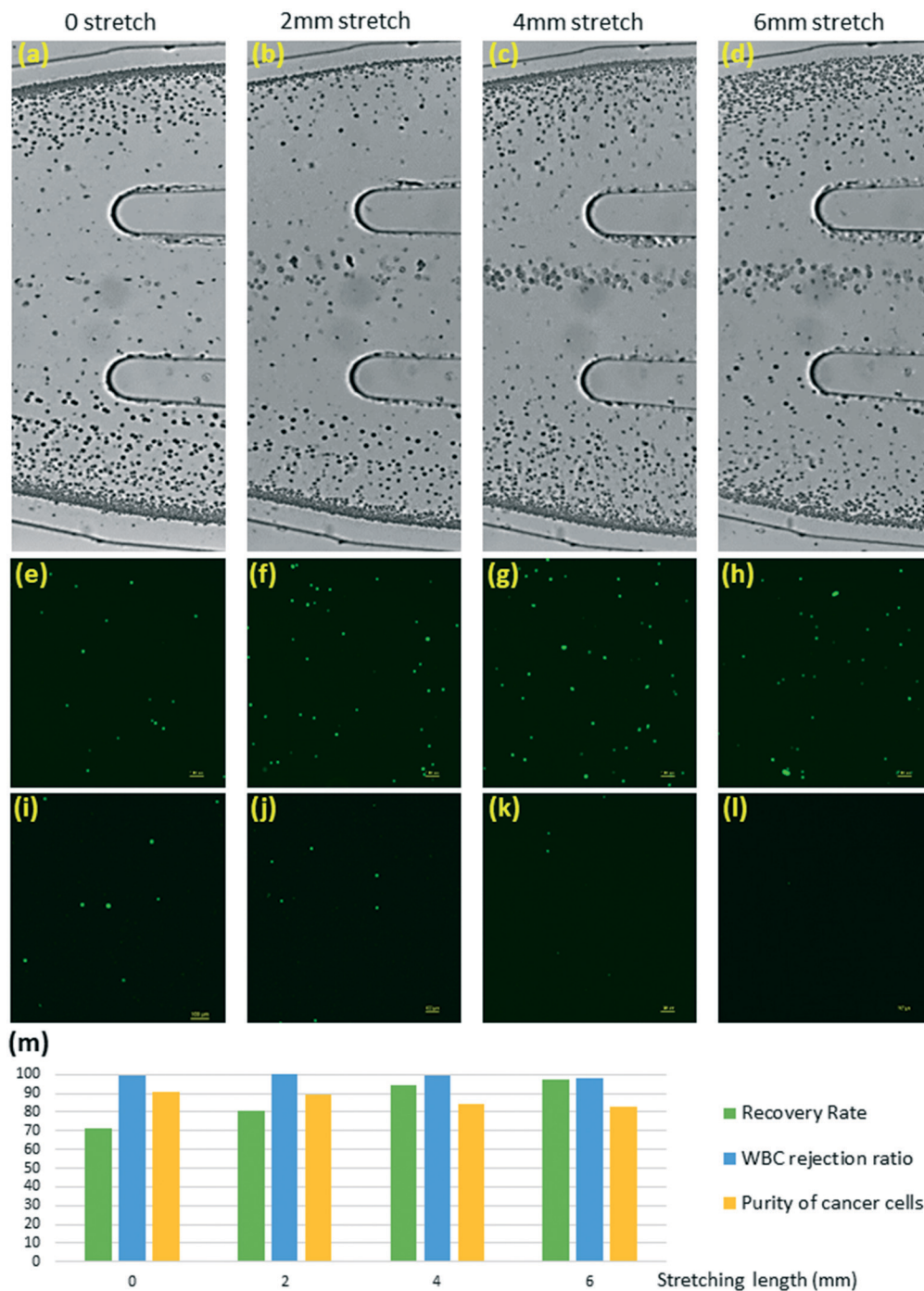


Fig. 5 Cancer cell isolation from WBCs in an elongated 10 mm channel. (a–d) Bright field images of the trifurcation region under different elongations. Cancer cells focus to the middle outlet by stretching. (e–h) Fluorescence images of the stained cancer cells collected from the middle outlet. (i–l) Fluorescence images show the stained cancer cells collected from the side outlets. While the middle outlet gets enriched with the cancer cells under stretching, their numbers diminish in the side outlets. The scale bar on the fluorescence images represent 100 μm . (m) Recovery rate and purity of the cancer cells as well as the WBC rejection ratio.

Fig. 6a–d show stacked images of the trajectories under elongation and demonstrate the expected improvement in focusing and separation of cancer cells from diluted whole blood. Fluorescence images obtained from outputs of the centre outlet (Fig. 6e–h) and the side outlets (Fig. 6i–l) further verify the enrichment of cancer cells in the centre outlet as

well as their depletion in the side outlets. Fig. 6m illustrates the enhancement of the recovery rate of the cancer cells from 74.5% to 98.6%, an almost stable blood cell rejection ratio around 99.5%, and a slight reduction in the purity of the collected cancer cells from 95 to 90%. The results indicate that stretching improves the recovery rate of the cancer cells

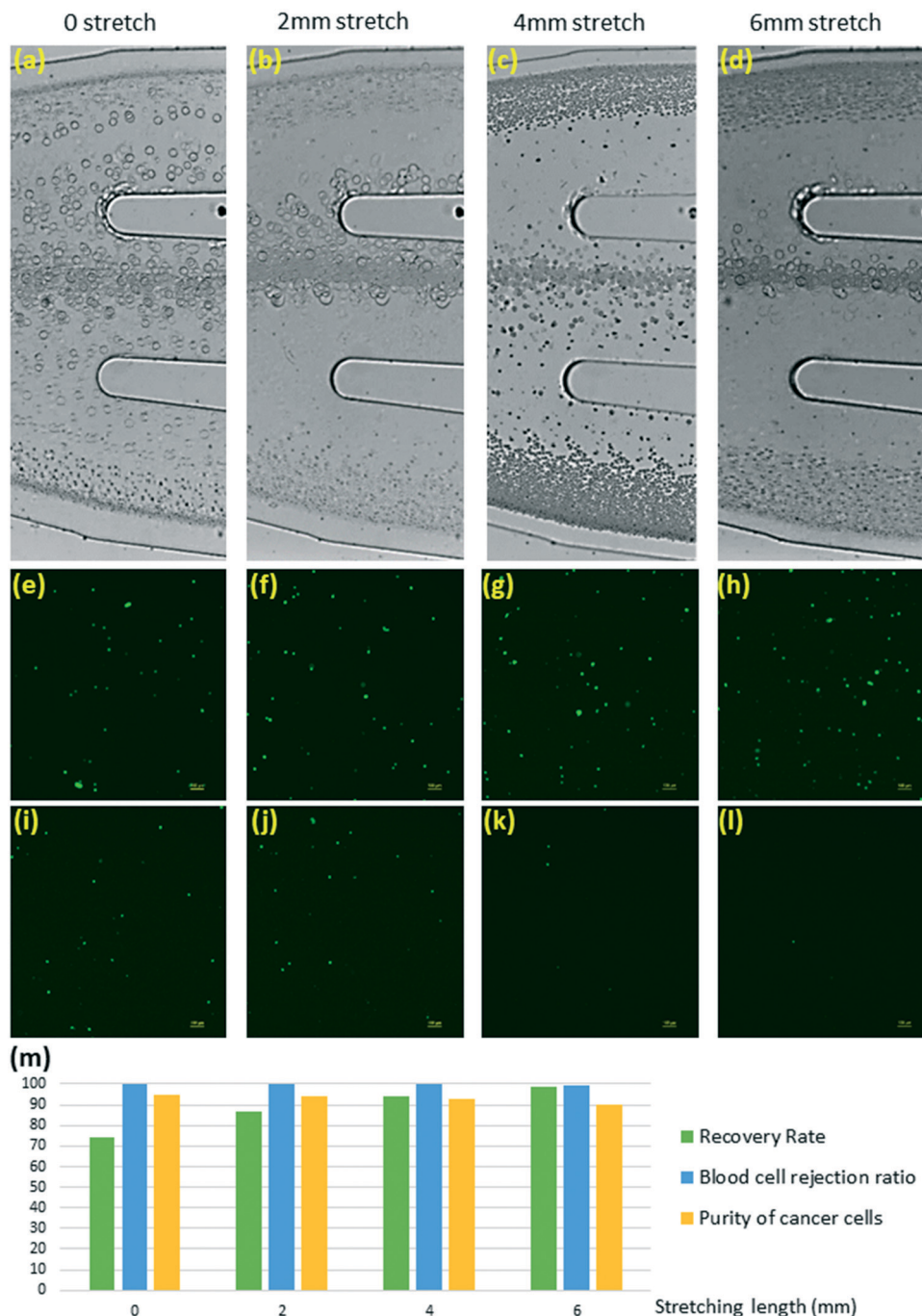


Fig. 6 Cancer cell isolation from diluted whole blood in an elongated 10 mm channel. (a–d) Bright field images of the trifurcation region of the channel under different elongations. While the blood cells are confined to the walls, cancer cells migrate toward the centre by stretching. (e–h) Fluorescence images of the stained cancer cells collected from the middle outlet. (i–l) Fluorescence images of the stained cancer cells collected from the side outlets. Fluorescence images verify the faster migration of cancer cells to the centre outlet under elongation. The scale bars in the fluorescence images represent 100 μm . (m) The recovery rate and purity of the cancer cells as well as the blood cell rejection ratio.

without compromising the purity significantly since the elongated channel and the reduced width facilitate the migration of the smaller cancer cells to the centre, while the blood cells are still at the sides. Thus, slight changes in dimension can be achieved with a minute amount of elongation of the microfluidic device. Comparing the bright field images of Fig. 5 and 6 further reveals that the blood

cells in Fig. 6 are more compactly confined to the sides, while in Fig. 5 they are less condensed and are closer to the boundary between the sides and the middle of the channel. This observation results from the size differences of WBCs and RBCs. WBCs are larger in size and elongation helps them to focus closer to the centre. Whereas, RBCs are much smaller, and 6 mm elongation is far less than enough to be

able to assist their migration closer to the centre channel. This also explains why the purity level was not markedly reduced for cancer cells in diluted blood. It should be noted that the ratio of CTCs to blood cells in real clinical samples is much smaller (1–10 CTCs in 1 mL whole blood) than that tested in this work. Nevertheless, this work serves as a proof of concept, demonstrating the size-tuneable separation capability of a stretchable device for biological applications.

Conclusions

In summary, we demonstrated a new scheme for achieving a tuneable separation of cells and particles of varied and wide size distributions using a stretchable inertial microfluidic system. Operating based on the deformability of stretchable microfluidics, our system proved that the elongation of microchannels can control the separation cut-off size of the device as well as increasing the separation resolution, leading to an onsite manageable isolation of particle/cell sizes of interest in a heterogenous mixture. We first quantified the reduction of cut-off size using a mixture of continuous sized particles of 2–26 μm . Then, we investigated the focusing and flow behaviour of T47D cancer cells and WBCs in an elongated microchannel, respectively. The results showed that the focusing efficiency of the cancer cells were improved and that the WBCs were mostly confined to the sides under the elongation with very slight contamination of the target outlet. We also showed that our system effectively isolated the target cells that had size overlap with the non-target cells without compromising the purity. Therefore, T47D cancer cell isolation from WBCs was achieved in our stretching platform and gave rise to promising results with recovery rate of 97.4% and purity of 82.6% for 6 mm elongation of the chip. Our platform is also suitable for a reliable isolation of cancer cells from diluted whole blood, leading to a high recovery rate of 98.6% and a high purity of 90% for T47D cancer cells. With the promising opportunities in stretchable microfluidics, the proposed platform is expected to facilitate the isolation and separation of cells and microparticles in terms of flexibility, onsite tunability, and real time optimization. Finally, we believe that the proposed stretchable microfluidic platform will have a broad application in biomedicine and further work could be done to enable additional degrees of stretching and subsequently more dimensional changes to be conducted onsite.

Author contributions

HF fabricated the devices, prepared the samples, carried out the experiments and evaluated the data and wrote the paper. NTN developed the concept, supervised the project, and wrote the paper. JZ supervised the experiments and evaluated the data. HPP edited the manuscript. SY cultured the cancer cells. HT provided the whole blood.

Conflicts of interest

There are no conflicts to declare.

Acknowledgements

Hedieh Fallahi acknowledges the support of the higher degree research scholarship from Griffith University. Nam-Trung Nguyen acknowledges the support from the Australian Research Council (ARC) Discovery Project (Grant No. DP180100055) and access to the Queensland node at Griffith of the Australian National Fabrication Facility, a company established under the National Collaborative Research Infrastructure Strategy to provide nano- and microfabrication facilities for Australia's researchers. Jun Zhang acknowledges the support from the Griffith University New Research Grant 2020 and Australian Research Council (ARC) DECRA fellowship (Grant No. DE210100692).

References

- 1 V. Akpe, T. H. Kim, C. L. Brown and I. E. Cock, *J. R. Soc., Interface*, 2020, **17**, 20200065.
- 2 M. G. Krebs, R. L. Metcalf, L. Carter, G. Brady, F. H. Blackhall and C. Dive, *Nat. Rev. Clin. Oncol.*, 2014, **11**, 129–144.
- 3 C. Burz, V.-V. Pop, R. Buiga, S. Daniel, G. Samasca, C. Aldea and I. Lupan, *Oncotarget*, 2018, **9**, 24561–24571.
- 4 P. Rostami, N. Kashaninejad, K. Moshksayan, M. S. Saidi, B. Firoozabadi and N.-T. Nguyen, *J. Sci.: Adv. Mater. Devices*, 2019, **4**, 1–18.
- 5 M. Umer, R. Vaidyanathan, N.-T. Nguyen and M. J. A. Shiddiky, *Biotechnol. Adv.*, 2018, **36**, 1367–1389.
- 6 N. Soda, B. H. A. Rehm, P. Sonar, N.-T. Nguyen and M. J. A. Shiddiky, *J. Mater. Chem. B*, 2019, **7**, 6670–6704.
- 7 M. C. Miller, G. V. Doyle and L. W. M. M. Terstappen, *J. Oncol.*, 2010, **2010**, 617421.
- 8 M. Ilie, V. Hofman, E. Long-Mira, E. Selva, J.-M. Vignaud, B. Padovani, J. Mouroux, C.-H. Marquette and P. Hofman, *PLoS One*, 2014, **9**, e111597.
- 9 K. E. Effenberger, C. Schroeder, A. Hanssen, S. Wolter, C. Eulenburg, M. Tachezy, F. Gebauer, J. R. Izbicki, K. Pantel and M. Bockhorn, *Clin. Cancer Res.*, 2018, **24**, 2844–2850.
- 10 J. C. Ahn, P.-C. Teng, P.-J. Chen, E. Posadas, H.-R. Tseng, S. C. Lu and J. D. Yang, *Hepatology*, 2020, **73**, 422–436.
- 11 W.-T. Yan, X. Cui, Q. Chen, Y.-F. Li, Y.-H. Cui, Y. Wang and J. Jiang, *Sci. Rep.*, 2017, **7**, 43464.
- 12 F. Castro-Giner and N. Aceto, *Genome Med.*, 2020, **12**, 31.
- 13 M. G. Krebs, J.-M. Hou, T. H. Ward, F. H. Blackhall and C. Dive, *Ther. Adv. Med. Oncol.*, 2010, **2**, 351–365.
- 14 J. Zhou, A. Kulasinghe, A. Bogseth, K. O'Byrne, C. Punyadeera and I. Papautsky, *Microsyst. Nanoeng.*, 2019, **5**, 8.
- 15 R. Guglielmi, Z. Lai, K. Raba, G. van Dalum, J. Wu, B. Behrens, A. A. S. Bhagat, W. T. Knoefel, R. P. L. Neves and N. H. Stoecklein, *Sci. Rep.*, 2020, **10**, 20312.
- 16 Y.-H. Chen, A. K. Pulikkathodi, Y.-D. Ma, Y.-L. Wang and G.-B. Lee, *Lab Chip*, 2019, **19**, 618–625.

- 17 A. Abdulla, T. Zhang, K. Z. Ahmad, S. Li, J. Lou and X. Ding, *Anal. Chem.*, 2020, **92**, 16170–16179.
- 18 H.-Y. Liu, C. Koch, A. Haller, S. A. Joosse, R. Kumar, M. J. Vellekoop, L. J. Horst, L. Keller, A. Babayan, A. V. Failla, J. Jensen, S. Peine, F. Keplinger, H. Fuchs, K. Pantel and M. Hirtz, *Adv. Biosyst.*, 2020, **4**, 1900162.
- 19 M. Yu, S. Stott, M. Toner, S. Maheswaran and D. A. Haber, *J. Cell Biol.*, 2011, **192**, 373–382.
- 20 Z. Lin, G. Luo, W. Du, T. Kong, C. Liu and Z. Liu, *Small*, 2020, **16**, 1903899.
- 21 L. Sun, W. Yang, S. Cai, Y. Chen, H. Chu, H. Yu, Y. Wang and L. Liu, *Biomed. Microdevices*, 2020, **22**, 55.
- 22 D. Hu, H. Liu, Y. Tian, Z. Li and X. Cui, *ACS Comb. Sci.*, 2020, **22**, 701–711.
- 23 X. Wei, K. Chen, S. Guo, W. Liu and X.-Z. Zhao, *ACS Appl. Bio Mater.*, 2021, **4**, 1140–1155.
- 24 J. Zhang, S. Yan, D. Yuan, G. Alici, N.-T. Nguyen, M. Ebrahimi Warkiani and W. Li, *Lab Chip*, 2016, **16**, 10–34.
- 25 W. Tang, S. Zhu, D. Jiang, L. Zhu, J. Yang and N. Xiang, *Lab Chip*, 2020, **20**, 3485–3502.
- 26 J. Sun, M. Li, C. Liu, Y. Zhang, D. Liu, W. Liu, G. Hu and X. Jiang, *Lab Chip*, 2012, **12**, 3952–3960.
- 27 M. E. Warkiani, G. Guan, K. B. Luan, W. C. Lee, A. A. S. Bhagat, P. Kant Chaudhuri, D. S.-W. Tan, W. T. Lim, S. C. Lee, P. C. Y. Chen, C. T. Lim and J. Han, *Lab Chip*, 2014, **14**, 128–137.
- 28 H. W. Hou, M. E. Warkiani, B. L. Khoo, Z. R. Li, R. A. Soo, D. S.-W. Tan, W.-T. Lim, J. Han, A. A. S. Bhagat and C. T. Lim, *Sci. Rep.*, 2013, **3**, 1259.
- 29 M. G. Lee, J. H. Shin, C. Y. Bae, S. Choi and J.-K. Park, *Anal. Chem.*, 2013, **85**, 6213–6218.
- 30 A. J. Mach, J. H. Kim, A. Arshi, S. C. Hur and D. Di Carlo, *Lab Chip*, 2011, **11**, 2827–2834.
- 31 J. Che, A. J. Mach, D. E. Go, I. Talati, Y. Ying, J. Rao, R. P. Kulkarni and D. Di Carlo, *PLoS One*, 2013, **8**, e78194.
- 32 E. Sollier, D. E. Go, J. Che, D. R. Gossett, S. O'Byrne, W. M. Weaver, N. Kummer, M. Rettig, J. Goldman, N. Nickols, S. McCloskey, R. P. Kulkarni and D. Di Carlo, *Lab Chip*, 2014, **14**, 63–77.
- 33 E. Ozkumur, A. M. Shah, J. C. Ciciliano, B. L. Emmink, D. T. Miyamoto, E. Brachtel, M. Yu, P.-i. Chen, B. Morgan, J. Trautwein, A. Kimura, S. Sengupta, S. L. Stott, N. M. Karabacak, T. A. Barber, J. R. Walsh, K. Smith, P. S. Spuhler, J. P. Sullivan, R. J. Lee, D. T. Ting, X. Luo, A. T. Shaw, A. Bardia, L. V. Sequist, D. N. Louis, S. Maheswaran, R. Kapur, D. A. Haber and M. Toner, *Sci. Transl. Med.*, 2013, **5**, 179ra147.
- 34 J. Zhou, C. Tu, Y. Liang, B. Huang, Y. Fang, X. Liang, I. Papautsky and X. Ye, *Sci. Rep.*, 2018, **8**, 9411.
- 35 J. Zhou and I. Papautsky, *Lab Chip*, 2013, **13**, 1121–1132.
- 36 A. Bogseth, J. Zhou and I. Papautsky, *Micromachines*, 2020, **11**, 287.
- 37 J. Zhou and I. Papautsky, *Lab Chip*, 2019, **19**, 3416–3426.
- 38 D. Lee, Y.-h. Choi and W. Lee, *Lab Chip*, 2020, **20**, 2861–2871.
- 39 D. Lee, S. M. Nam, J.-a. Kim, D. Di Carlo and W. Lee, *Anal. Chem.*, 2018, **90**, 2902–2911.
- 40 Y. Zhou, Z. Ma and Y. Ai, *Lab Chip*, 2020, **20**, 568–581.
- 41 J. Zhou and I. Papautsky, *Microsyst. Nanoeng.*, 2020, **6**, 113.
- 42 H. Fallahi, J. Zhang, J. Nicholls, H.-P. Phan and N.-T. Nguyen, *Anal. Chem.*, 2020, **92**, 12473–12480.
- 43 H. Fallahi, J. Zhang, H.-P. Phan and N.-T. Nguyen, *Micromachines*, 2019, **10**, 830.
- 44 N.-T. Nguyen, *Micromachines*, 2020, **11**, 1004.
- 45 S. Yadav, R. Vadivelu, M. Ahmed, M. Barton and N.-T. Nguyen, *Exp. Cell Res.*, 2019, **378**, 191–197.
- 46 S. Yadav, M. Barton and N.-T. Nguyen, *Adv. Biosyst.*, 2020, **4**, 1900222.
- 47 S. Yadav, N. Kashaninejad and N.-T. Nguyen, *Micromachines*, 2020, **11**, 729.
- 48 J.-a. Kim, J.-R. Lee, T.-J. Je, E.-c. Jeon and W. Lee, *Anal. Chem.*, 2018, **90**, 1827–1835.
- 49 G. Guan, L. Wu, A. A. Bhagat, Z. Li, P. C. Y. Chen, S. Chao, C. J. Ong and J. Han, *Sci. Rep.*, 2013, **3**, 1475.
- 50 M. G. Lee, J. H. Shin, S. Choi and J.-K. Park, *Sens. Actuators, B*, 2014, **190**, 311–317.
- 51 X. Wang and I. Papautsky, *Lab Chip*, 2015, **15**, 1350–1359.
- 52 J. Zhou, P. V. Giridhar, S. Kasper and I. Papautsky, *Lab Chip*, 2013, **13**, 1919–1929.